THE BELL SYSTEM TECHNICAL JOURNAL
Vol. 55, No. 3, March 1976
Printed in U. S. A.

Cross Polarization in Reflector-Type Beam Waveguides and Antennas

By M. J. GANS

(Manuscript received October 29, 1975)

Using the paraxial ray approximation, simple formulas for the cross polarization introduced by curved reflectors are developed. In particular, when the reflectors are quadric surfaces of revolution with the center ray of the beam passing through the foci, the maximum cross-polarized field amplitude throughout a gaussian beam, relative to the on-axis copolarized field, is

$$C = \frac{2\xi\kappa_\perp}{\sqrt{e}} \sin\theta_i,$$

where e is the base of the natural logarithm, ξ is the 1/e power radius of the beam, $\kappa_\perp$ is the curvature of the reflector perpendicular to the plane of incidence, and θ_i is the angle of incidence. For such reflectors, the beam fields are accurately represented by a superposition of just two gaussian modes for each plane of polarization: the fundamental mode, which corresponds to the co-polarized gaussian beam, and a higher-order mode, which accounts for the cross-polarized field and the amplitude "space" taper. Transformation of a beam through a general sequence of such reflectors is influenced by three factors: the curved reflectors, longitudinal propagation lengths, and rotations of the plane of incidence. The effect of each factor is described by a 4 × 4 matrix relating the input and output gaussian modes. Several typical beam-reflector systems are analyzed by this method. Theoretical cross-polarization patterns are shown to be in accurate agreement with measurements on a symmetrical dual-reflector system.

I. INTRODUCTION

At millimeter wavelengths, normal waveguide losses become too large in many applications. For example, long lengths of waveguide are required in satellite earth stations between the transceiver and the reflector antenna focus. To reduce these losses one may use quasi-optical beams[1] which employ reflectors or lenses for refocusing at various intervals, thereby confining the beam within a geometric tube with no (lossy) guiding walls. Long-focal-length, multiple-reflector

antennas (e.g., Cassegrainian and Gregorian antennas) may themselves be thought of in the context of beam waveguides.

In another application, periodically refocussed beams of millimeter or submillimeter wavelength electromagnetic waves might be used[2] as a means of distributing large amounts of information in cities. Such a transmission system is referred to as Hertzian cable.

In the above beam waveguide systems, it is desirable to double the system capacity by transmitting separate signals on each of two orthogonal polarizations (e.g., vertical and horizontal linear polarizations). In such dual-polarization systems, cross-polarization coupling introduced by the refocusers can significantly decrease system performance because of crosstalk between the different signals carried on each of the two polarizations.

The purpose of this paper is to describe simple formulas for computing the cross-polarization coupling introduced by sequences of beam refocusers which consist of quadric reflector surfaces arranged with the beam axis passing through their foci.

II. CROSS POLARIZATION OWING TO REFLECTOR CURVATURE

Consider a beam incident on a flat reflector, as in Fig. 1a. We restrict our attention to beams with narrow angular divergence where the paraxial ray approximation applies so that, for example, the beam field may be described in terms of gaussian beam modes.[3] The paraxial ray approximation applies roughly whenever the 3-dB angular divergence of the beam is less than one radian.

The geometrical optics law of reflection from a perfect conductor is*

$$\hat{e}_r = 2\hat{n}(\hat{n}\cdot\hat{e}_i) - \hat{e}_i, \tag{1}$$

where $\hat{e}_i$ and $\hat{e}_r$ are unit vectors in the direction of the incident and reflected field polarizations, respectively, and $\hat{n}$ is the surface unit normal vector. The caret "^" indicates a unit vector. If the polarization of the incident field is a fixed linear polarization throughout the beam and is perpendicular to the surface normal, then

$$\hat{e}_r = -\hat{e}_i; \tag{2}$$

i.e., the reflected field is also a fixed linear polarization throughout the beam. As expected, a flat plate introduces no cross polarization.

In general, a reflector will be curved with two principal radii of curvature,[4] as shown in Fig. 1b. The surface unit normal vector will no longer be perpendicular to $\hat{e}_i$ at all points. In fact, for small displacements Δx and Δy along the directions of maximum and minimum

* See Ref. 9, Sec. 6.11, for example.

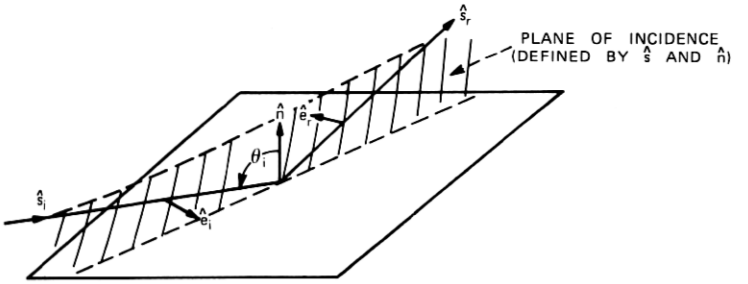

(a)

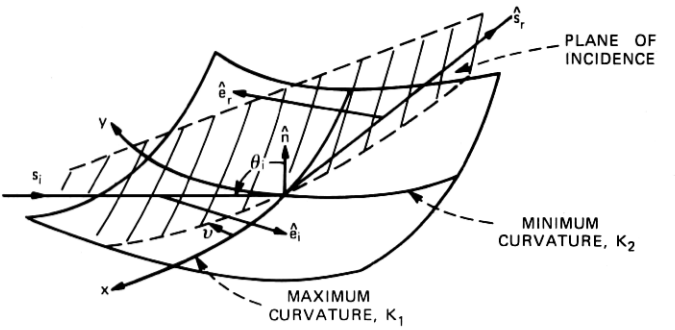

(b)

Fig. 1—(a) Reflection of a beam from a flat plate. (b) Reflection of a beam from a curved surface.

curvature, respectively, the unit normal vector will change by

$$\Delta\hat{n} = -\kappa_1(\Delta x)\hat{x} - \kappa_2(\Delta y)\hat{y}, \tag{3}$$

where κ_1 and κ_2 are the maximum and minimum curvatures, respectively, and positive curvature indicates the surface bends toward the incident radiation.

This change in the surface unit normal vector causes the term $(\hat{n}\cdot\hat{e}_i)$ in eq. (1) to change from zero to

$$(\hat{n}\cdot\hat{e}_i) = -\kappa_1(\Delta x)\sin\nu + \kappa_2(\Delta y)\cos\nu, \tag{4}$$

where ν is the angle between the plane of incidence and the direction of maximum curvature as shown in Fig. 1b.

Thus, due to surface curvature, the polarization of the reflected field varies over the surface from that resulting from a flat plate $(-\hat{e}_i)$ by an additional component $2\hat{n}(\hat{n}\cdot\hat{e}_i)$. Part of this component represents the change in the in-line polarization as a consequence of the change in the reflected-ray direction, and part represents cross-polarized signal

introduced by the surface curvature. The portion of $\hat{n}$ that is aligned with the cross-polarized field (the field in the plane of incidence and perpendicular to the reflected ray) is of magnitude $\sin \theta_i$. Thus, the ratio of the cross-polarized field to the incident field at a given point is

$$c = 2 \sin \theta_i[-\kappa_1(\Delta x) \sin \nu + \kappa_2(\Delta y) \cos \nu] \tag{5}$$

or

$$c = -2(\Delta\rho) \sin \theta_i \sqrt{(\kappa_1 \sin \nu)^2 + (\kappa_2 \cos \nu)^2} \cos (\phi + \sigma), \tag{6}$$

where

$$\sigma = \arctan\left(\frac{\kappa_2}{\kappa_1} \cot \nu\right).$$

$\Delta\rho$ is the displacement of the reflection point from that of the beam center and ϕ is the angular direction of that displacement relative to the axis of maximum curvature. For a fixed displacement, $\Delta\rho$, the direction, ϕ, that gives maximum cross-polarized signal ratio, c, is $\phi_{\max} = -\sigma$.

If one assumes the incident polarization is in the plane of incidence rather than perpendicular to the plane of incidence, the resulting cross-polarized field is also found to be given by eqs. (5) and (6).

If the incident beam has a gaussian amplitude distribution

$$E_i = E_0 \exp\left\{-\frac{(\Delta\rho)^2}{2\xi^2}[1 - \sin^2 \theta_i \cos^2 (\phi - \nu)]\right\} \tag{7}$$

(where ξ is the $1/e$ beam intensity radius), one may calculate the ratio of the cross-polarized field relative to the in-line on-axis field (denoted by capital C to differentiate from the lower case c, representing the ratio of in-line and cross-polarized fields at the same point),

$$C = -2(\Delta\rho) \sin \theta_i \sqrt{(\kappa_1 \sin \nu)^2 + (\kappa_2 \cos \nu)^2} \cos (\phi + \sigma) \exp\left\{-\frac{(\Delta\rho)^2}{2\xi^2}[1 - \sin^2 \theta_i \cos^2 (\phi - \nu)]\right\}. \tag{8}$$

For a fixed direction ϕ, the radius $\Delta\rho$ at which the relative cross polarization is maximum is

$$\Delta\rho_{C_{\max}} = \frac{\xi}{\sqrt{1 - \sin^2 \theta_i \cos^2 (\phi - \nu)}}, \tag{9}$$

with

$$C_{\max} = -\frac{2\xi \sin \theta_i \sqrt{(\kappa_1 \sin \nu)^2 + (\kappa_2 \cos \nu)^2}}{\sqrt{e}\sqrt{1 - \sin^2 \theta_i \cos^2 (\phi - \nu)}} \cos (\phi + \sigma), \tag{10}$$

and the direction, $\phi_{C_{\max}}$, which provides the greatest cross polarization,

is given by

$$\phi_{C_{\max}} = \arctan\left[\frac{\sin^2\theta_i \sin(\nu+\sigma)\cos(\nu+\sigma)}{1-\sin^2\theta_i \sin^2(\nu+\sigma)}\right] - \sigma. \quad (11)$$

When the plane of incidence coincides with either of the principal curvature planes ($\nu = 0°$ or $90°$), as in the case of quadric surfaces with the beam center ray passing through the surface foci, the expression for the maximum cross polarization of eq. (10) simplifies to

$$\boxed{C_{\max} = \frac{2\xi}{\sqrt{e}}\kappa_\perp \sin\theta_i} \quad (12)$$

(plane of incidence coincides with either plane of principal curvature), where $\kappa_\perp$ is the curvature in the direction normal to the plane of incidence. Thus, in this case, the maximum cross-polarized field is found in a direction normal to the plane of incidence in the direction of maximum (if $\nu = 0°$) or minimum (if $\nu = 90°$) surface curvature.

In one example, an antenna is formed from two cylindrical mirrors such that $\nu = 0°$ and $\kappa_\perp = 0$ for both mirrors, which by eq. (12) indicates that no cross polarization is generated by the mirrors, in agreement with the results of Ref. 5.

Another example is the offset paraboloid launcher, shown in Fig. 2. The maximum cross-polarization amplitude ratio was derived in Ref. 6 and found to be

$$C_{\max} = \frac{\theta_e \tan(\theta_0/2)}{\sqrt{e}\ln 10}, \quad (13)$$

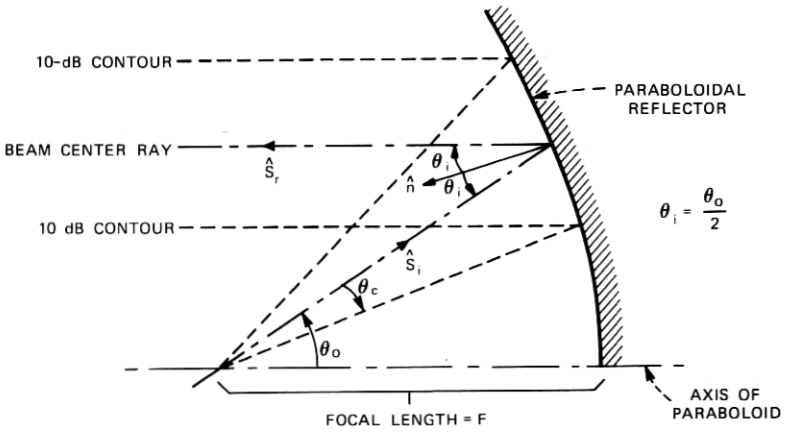

Fig. 2—Offset paraboloid launcher.

where θ_c is the 10-dB half angle of the gaussian beam incident from the focus and θ_0 is the offset angle of the beam center ray.

The $1/e$ beam intensity radius ξ at the paraboloidal reflector is related to the 10-dB half angle, θ_c, by

$$\xi = \frac{\theta_c F \sec^2 (\theta_0/2)}{\sqrt{\ln 10}}; \qquad \theta_0 = 2\theta_i, \tag{14}$$

where F is the focal length of the paraboloid. The curvature of the paraboloid in the direction perpendicular to the plane of incidence is

$$\kappa_\perp = \frac{\cos (\theta_0/2)}{2F}. \tag{15}$$

Using eqs. (14) and (15), it is seen that eq. (12) is in agreement with eq. (13).

Another example is the use of cylindrical mirrors in Hertzian cable systems. A typical refocuser mirror arrangement[7] is shown in Fig. 3. The beam remains in a horizontal plane (the plane of incidence) as it is refocused by two cylindrical mirrors both tilted so that their direction of curvature makes an angle $\nu = 50.5$ degrees with the plane of incidence. The output beam has changed direction from the input beam by 225 degrees. The angle of incidence at both mirrors is 33.75 degrees and the curvatures are

$$\kappa_2 = 0,$$

$$\kappa_1 = \frac{1}{66} \text{ meters}^{-1},$$

and the beam radius is

$$\xi = 0.212 \text{ meters}.$$

The tilted orientation of the mirrors allows the mirrors to have equal curvature and large aperture efficiency while maintaining sharp focusing and beam symmetry.[7]

The maximum cross polarization for the pair of reflectors is less than twice the maximum cross polarization from either one of the reflectors alone. From eq. (6), σ is zero, and from eq. (11)

$$\phi_{c_{max}} = 10.515 \text{ degrees}.$$

From eq. (10) the maximum cross polarization is

$$20 \log_{10} (2C_{max}) = -48.4 \text{ dB}. \tag{16}$$

This is indeed a small value; however, in Hertzian cables with many such refocusers, this cross polarization could accumulate to be a problem.

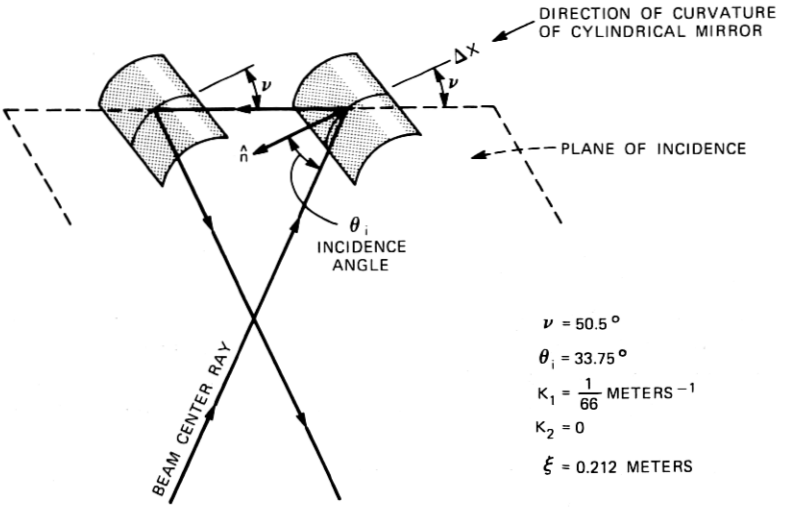

Fig. 3—Typical Hertzian cable refocuser-redirector.

By using geometric optics, eqs. (1) and (7), the cross polarization has been numerically computed for various ellipsoids and paraboloids. The maximum cross polarization was found by a trial-and-error search and compared with that predicted from the paraxial ray result, eq. (12). The comparisons indicate that eq. (12) is accurate to within 0.1 dB for 10-dB half angles of the beam less than 45 degrees.

III. DECOMPOSITION INTO GAUSSIAN BEAM MODES

As described in the previous section, with quadric surface mirrors and the beam center ray passing through the foci of the surfaces, the cross-polarized field resulting from reflection of a perfectly polarized incident gaussian beam is maximum in a direction perpendicular to the plane of incidence and has the maximum value, relative to the in-line polarized field on axis, given by eq. (12), at a distance ξ from the beam center ray.

It is shown in Ref. 6 that this type of reflected field can be represented as the superposition of two gaussian beam modes:[3]

(*i*) Fundamental mode

$$\mathbf{E}_{00} = (H_{00}\hat{x} + V_{00}\hat{y}) \frac{\sqrt{2\eta}}{\sqrt{\pi}\xi_{00}} \cdot \exp\left\{ - jkz - \frac{\rho^2}{2\xi_{00}^2} + j\left[\arctan\left(\frac{z}{k\xi_{00}^2} \right) - \frac{k\rho^2}{2R_{00}} \right] \right\}, \quad (17)$$

(*ii*) Higher-order mode

$$\mathbf{E}_{01} = [V_{01}(\hat{x}\cos\alpha - \hat{y}\sin\alpha) - H_{01}(\hat{x}\sin\alpha + \hat{y}\cos\alpha)]\frac{\sqrt{2\eta\rho}}{\sqrt{\pi}\xi_{01}^2}$$

$$\cdot\exp\left\{-jkz - \frac{\rho^2}{2\xi_{01}^2} + j\left[2\arctan\left(\frac{z}{k\bar{\xi}_{01}^2}\right) - \frac{k\rho^2}{2R_{01}}\right]\right\}, \quad (18)$$

where η is the free-space impedance, $\sqrt{\mu_0/\epsilon_0}$, and V_{00}, H_{00}, and V_{01}, H_{01} are the phasor coefficients of the fundamental and higher-order gaussian beam fields for the cases when the incident electric field is in the plane of incidence (V) and perpendicular to the plane of incidence (H), respectively. The subscripts refer to the standard TEM_{00} and TEM_{01} mode notations of Ref. 8, not the "m" and "n" of Ref. 3. $\hat{y}$ and $\hat{x}$ are unit vectors normal to the beam axis in the plane of incidence and normal to the plane of incidence, respectively; ρ, α, and z are cylindrical coordinates, with z denoting distance along the beam axis from the beam waist.

At the beam waist, $z = 0$, the radius of curvature of the phase front of the beam field, R, is infinite, and the field varies with increasing distance, ρ, from the axis at a rate determined by $\bar{\xi}$. For the fundamental mode, the field is maximum on axis and decreases to $1/\sqrt{e}$ of its maximum value at $\rho = \bar{\xi}_{00}$. For the higher-order mode, the field is maximum at $\rho = \bar{\xi}_{01}$ and decreases to $\sqrt{2/e}$ of its maximum value at $\rho = \sqrt{2}\bar{\xi}_{01}$. Away from the beam waist $z \neq 0$, the beam-field amplitude varies with ρ at a rate determined by ξ instead of $\bar{\xi}$, and the phase front has a finite radius of curvature R. ξ and R are determined from $\bar{\xi}$ and z by the following formulas:[8]

$$\xi = \bar{\xi}\sqrt{1 + \left(\frac{z}{k\bar{\xi}^2}\right)^2} \quad (19)$$

and

$$R = z\left[1 + \left(\frac{k\bar{\xi}^2}{z}\right)^2\right]. \quad (20)$$

The choice of eq. (18) as the higher-order mode is based[6] on its ability to approximate simultaneously both the cross-polarization and the "space" taper (amplitude asymmetry from top to bottom of mirror) properties of offset reflectors.

Both modes have a characteristic exponential attenuation with distance from axis, $\exp(-\rho^2/2\xi^2)$, and a spherical wavefront near the axis at constant z, denoted by the term, $\exp(-jk\rho^2/2R)$. As one passes through a beam waist, with increasing z, the on-axis phase advances by π for the fundamental mode and 2π for the higher-order mode (relative to the plane-wave retardation, e^{-jkz}). Thus, if the cross-

polarization field (due to the higher-order mode) is in phase with the in-line polarization field at the beam waist, it will be in phase quadrature at large distances, $z \gg k\xi$, from the beam waist.

From the results of Section II and eqs. (17) and (18), we find that, if the higher-order mode is generated by reflection with incidence angle, θ_i, from a quadric surface with curvature, κ_1, perpendicular to the plane of incidence, beam radius, ξ, and reflected phase front radius of curvature R at the reflector, then

$$\xi_{00}(z_r) = \xi_{01}(z_r) = \xi, \tag{21}$$

$$R_{00}(z_r) = R_{01}(z_r) = R, \tag{22}$$

and

$$\gamma \triangleq \frac{V_{01}}{V_{00}} = \frac{H_{01}}{H_{00}} = \sqrt{e}C_{\max} = 2\xi\kappa_1 \sin\theta_i, \tag{23}$$

where the reflector is at $z = z_r$, and the beam waist is at $z = 0$. A picture of a typical aperture-field decomposition into gaussian beam-mode fields is shown in Fig. 4.

Note that, at the reflector z_r, the two modes are in phase with equal beam radii and phase-front curvatures. As one progresses along the beam to an observation point, z_0, the beam radii and phase-front

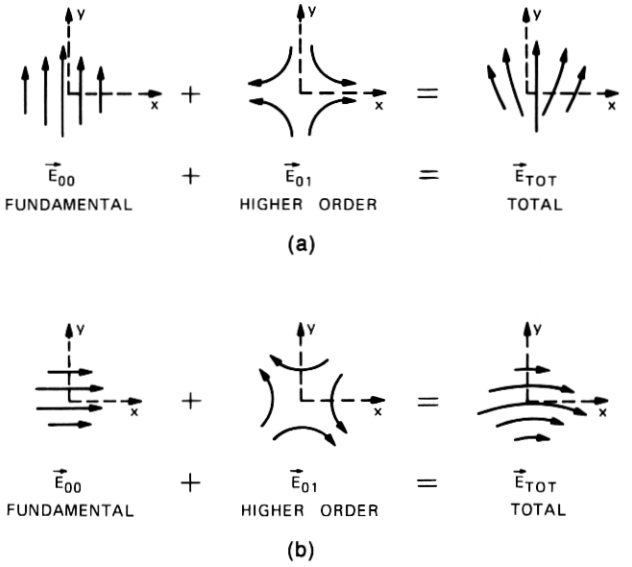

Fig. 4—Two-mode decomposition of aperture field (looking opposite to direction of propagation). (a) Feed horn vertically polarized (parallel to plane of incidence). (b) Feed horn horizontally polarized (perpendicular to plane of incidence).

curvature are still equal

$$\xi_{00}(z_0) = \xi_{00}(z_0) = \bar{\xi}\sqrt{1 + \left(\frac{z_0}{k\bar{\xi}^2}\right)^2} \tag{24}$$

and

$$R_{00}(z_0) = R_{01}(z_0) = z_0\left[1 + \left(\frac{k\bar{\xi}^2}{z_0}\right)^2\right], \tag{25}$$

where $\bar{\xi}$ and z_r are given by[8]

$$\bar{\xi} = \frac{\xi}{\sqrt{1 + (k\xi^2/R)^2}}, \tag{26}$$

and

$$z_r = \frac{R}{1 + (R/k\xi^2)^2}. \tag{27}$$

However, at z_0 there is a relative phase shift between the higher-order mode and the fundamental mode, from eqs. (17) and (18),

$$\Delta\Phi = \Phi_{01}(z_0) - \Phi_{00}(z_0) = \arctan\left(\frac{z_0}{k\bar{\xi}^2}\right) - \arctan\left(\frac{z_r}{k\bar{\xi}^2}\right). \tag{28}$$

This is the relative phase shift near the beam waist mentioned above. When the beam is focusing down towards the beam waist, R and z are negative; when diverging away from the beam waist, R and z are positive.

The power carried by each of the modes in terms of their mode phasors is

$$P = \int_0^\infty \rho d\rho \int_0^{2\pi} d\alpha \frac{|\mathbf{E}|^2}{2\eta} = |A|^2, \tag{29}$$

where A is the phasor of the particular mode in question; i.e., V_{00}, H_{00}, V_{01}, or H_{01}.

IV. MATRIX REPRESENTATION OF BEAM-WAVEGUIDE FACTORS

To keep track of the cross polarization generated by a sequence of factors in a beam-waveguide system, it is useful to represent each factor in terms of its transmission matrix[9] for the fundamental and higher-order modes. We will consider three types of factors that normally affect cross polarization in the reflection process: (*i*) the reflectors per se, (*ii*) the longitudinal propagation length, and (*iii*) the rotation of plane of incidence. See Fig. 5 for an example.

If ξ and R are the same for all modes at the input to a series of reflectors, they remain so throughout the system. Thus, we will assume ξ and R the same for all modes in what follows. If several modes are injected with different pairs of ξ and R, the response to each mode may

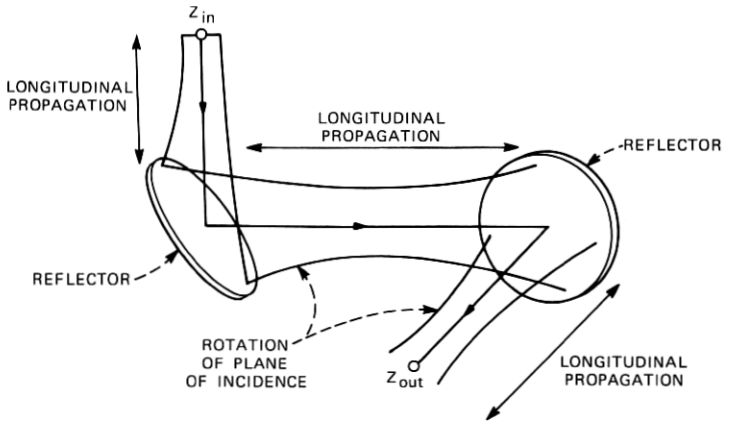

Fig. 5—Factors influencing cross polarization in a reflector-type beam system.

be computed as shown herein and then superposition used to find the total output.

As a dual-mode beam progresses along, undergoing a number of reflections, each factor may be thought of as a reflectionless, passive, eight-port device, as shown in Fig. 6. The coupling between the various modes may be expressed by the matrix equation

$$\mathbf{b} = \boldsymbol{T}\mathbf{a}, \tag{30}$$

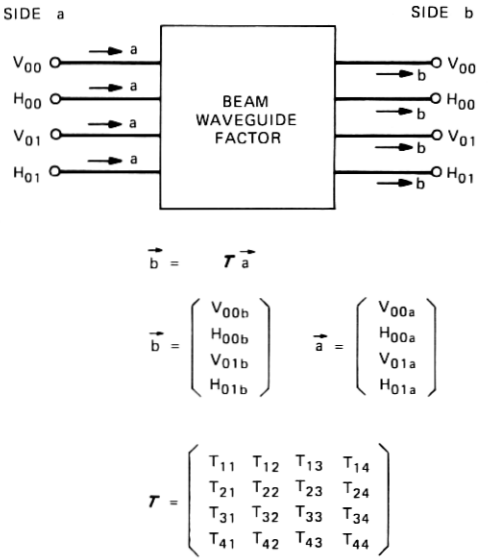

Fig. 6—The beam waveguide factor as a reflectionless eight port.

where **a** is a four vector whose components are the phasors of the input modes,

$$\mathbf{a} = \begin{bmatrix} V_{00a} \\ H_{00a} \\ V_{01a} \\ H_{01a} \end{bmatrix}, \tag{31}$$

and **b** is the four vector whose components are the phasors of the output modes

$$\mathbf{b} = \begin{bmatrix} V_{00b} \\ H_{00b} \\ V_{01b} \\ H_{01b} \end{bmatrix}. \tag{32}$$

The properties of the beam factor are described by the four-by-four factor matrix,

$$\boldsymbol{T} = \begin{bmatrix} T_{11} & T_{12} & T_{13} & T_{14} \\ T_{21} & T_{22} & T_{23} & T_{24} \\ T_{31} & T_{32} & T_{33} & T_{34} \\ T_{41} & T_{42} & T_{43} & T_{44} \end{bmatrix}. \tag{33}$$

In general, the matrix $\boldsymbol{T}$ depends on the parameters of the beam propagating through the system. However, it is a simple matter to compute the appropriate matrix for each beam and beam direction one wishes to apply to the system.

4.1 Curved-reflector matrix

To express the beam modes in a form which allows the reflectors to be oriented arbitrarily in space, the beam coordinates at the input and output of a reflector are defined with z in the direction of propagation, y in the plane of incidence perpendicular to z and toward the surface normal, and x normal to z and y (thus normal to the plane of incidence) so that (x, y, z) forms a right-handed cartesian coordinate system, as shown in Fig. 7.

By using the cross-polarization analysis of Section II, the mode definitions of Section III, and conservation of power, the matrix elements applying when a fundamental mode is incident are easily determined:

$$\left.\begin{aligned} &T_{11} = \sqrt{1 - \gamma^2}, \quad T_{13} = -\gamma, \quad T_{22} = -\sqrt{1 - \gamma^2}, \quad T_{24} = \gamma, \\ &T_{12} = T_{21} = T_{14} = T_{23} = 0, \end{aligned}\right\} \tag{34}$$

where γ is given in eq. (23) as $2\xi\kappa_\perp \sin\theta_i$. Note that, for reflectors concave or convex in the direction perpendicular to the plane of incidence, γ is positive or negative, respectively.

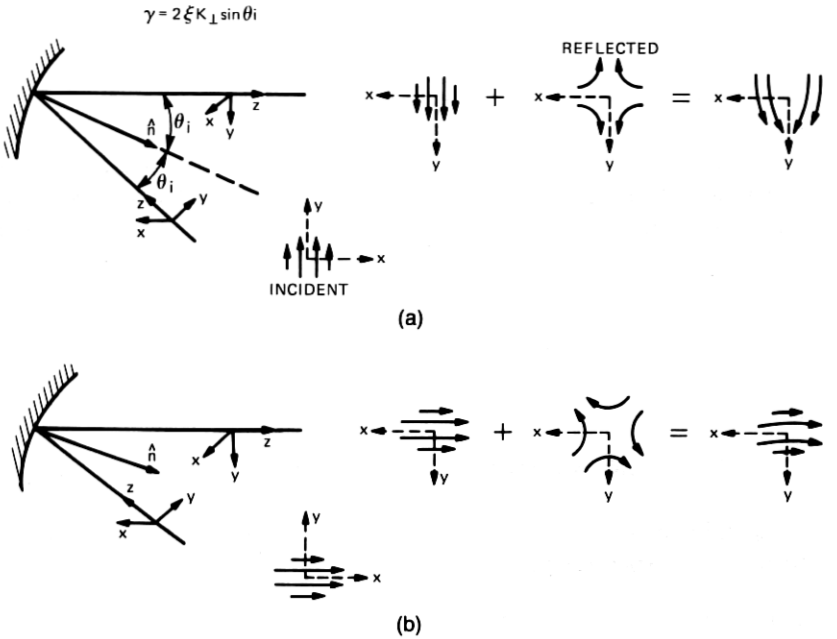

Fig. 7—Reflector matrix components (fields viewed in direction opposite to propagation direction). (a) V_{00} incident. (b) H_{00} incident.

Since the complex conjugate electric field satisfies Maxwell's equations and the boundary conditions on a perfect conductor (time reversal symmetry), the remaining matrix elements follow readily from the above real matrix elements of eq. (34):

$$\left.\begin{aligned} &T_{33} = -\sqrt{1-\gamma^2}, \quad T_{31} = -\gamma, \quad T_{44} = \sqrt{1-\gamma^2}, \quad T_{42} = \gamma, \\ &T_{41} = T_{32} = T_{43} = T_{34} = 0. \end{aligned}\right\} \tag{35}$$

Note that V modes (plane-of-incidence modes) do not couple to H modes (normal-to-plane-of-incidence modes) during reflection from a curved reflector. Thus we have

$$\boldsymbol{T}_{\text{ref}} = \begin{bmatrix} \sqrt{1-\gamma^2} & 0 & -\gamma & 0 \\ 0 & -\sqrt{1-\gamma^2} & 0 & \gamma \\ -\gamma & 0 & -\sqrt{1-\gamma^2} & 0 \\ 0 & \gamma & 0 & \sqrt{1-\gamma^2} \end{bmatrix}. \tag{36}$$

Since the matrix only describes transmission one way, the matrix elements are not necessarily directly related by reciprocity.

4.2 Longitudinal-propagation matrix

As mentioned in Section II, there is a relative phase shift between higher-order modes and their corresponding fundamental modes. In analyzing beam propagation through a system, it is only required to keep track of the relative mode phases to compute the overall cross-polarization coupling. Thus, we will lump all the differential beam-waist phase shifts, $\Delta\Phi$, of eq. (28) with the higher-order modes. As a result, the beam-factor matrix for a longitudinal-propagation length l is

$$\boldsymbol{T}_{lp} = \begin{bmatrix} 1 & 0 & 0 & 0 \\ 0 & 1 & 0 & 0 \\ 0 & 0 & e^{+j\Delta\Phi} & 0 \\ 0 & 0 & 0 & e^{+j\Delta\Phi} \end{bmatrix}, \tag{37}$$

where

$$\Delta\Phi = \arctan\left(\frac{z_b}{k\bar{\xi}^2}\right) - \arctan\left(\frac{z_a}{k\bar{\xi}^2}\right), \tag{38}$$

and z_a and z_b are the positions, relative to the beam waist, of the input and output, respectively.

4.3 Rotation-of-plane-of-incidence matrix

As described in Section 4.1, the beam coordinates are attached to the plane of incidence of each reflector. Thus as one passes from one reflector to another, the plane of incidence may rotate, and what had been a plane-of-incidence mode (V mode) may become a normal-to-plane-of-incidence mode (H mode). From Fig. 4, if one rotates the plane of incidence clockwise by an angle β, the projections of the input modes onto the output modes give the following beam factor matrix for rotation of plane of incidence:

$$\boldsymbol{T}_{\text{rot}} = \begin{bmatrix} \cos\beta & -\sin\beta & 0 & 0 \\ \sin\beta & \cos\beta & 0 & 0 \\ 0 & 0 & \cos 2\beta & -\sin 2\beta \\ 0 & 0 & \sin 2\beta & \cos 2\beta \end{bmatrix}. \tag{39}$$

V. TYPICAL BEAM-WAVEGUIDE APPLICATIONS

In this section, we illustrate the application of the above formulas by considering some typical beam-reflector systems.

5.1 Symmetrical dual reflector

In the symmetrical dual-reflector configuration shown in Fig. 8a, there is no rotation of plane of incidence. The arrangement comprises a curved reflector, followed by a longitudinal propagation length, followed by another reflector. Thus the overall beam system matrix is

the product of three beam-factor matrices

$$\boldsymbol{T} = \boldsymbol{T}_{\text{ref }2}\boldsymbol{T}_{lp}\boldsymbol{T}_{\text{ref }1}, \tag{40}$$

where T_{ref} is given by eq. (36) and $\boldsymbol{T}_{lp}$ by eq. (37). Neglecting terms of order γ^2, we have

$$\boldsymbol{T} \doteq \begin{bmatrix} 1 & 0 & -\gamma_1 + e^{j\Delta\Phi}\gamma_2 & 0 \\ 0 & 1 & 0 & -\gamma_1 + e^{j\Delta\Phi}\gamma_2 \\ -\gamma_2 + e^{j\Delta\Phi}\gamma_1 & 0 & e^{j\Delta\Phi} & 0 \\ 0 & -\gamma_2 + e^{j\Delta\Phi}\gamma_1 & 0 & e^{j\Delta\Phi} \end{bmatrix}. \tag{41}$$

From eq. (41), we see that to avoid conversion from a fundamental mode input to a higher-order mode at the output,

$$e^{-j\Delta\Phi} = \frac{\gamma_1}{\gamma_2} = \frac{\xi_1\kappa_{\perp 1}\sin\theta_{i1}}{\xi_2\kappa_{\perp 2}\sin\theta_{i2}}, \tag{42}$$

which implies

$$\xi_1\kappa_{\perp 1}\sin\theta_{i1} = \xi_2\kappa_{\perp 2}\sin\theta_{i2}, \qquad \Delta\Phi = 0 \tag{43}$$

or

$$\xi_1\kappa_{\perp 1}\sin\theta_{i1} = -\xi_2\kappa_{\perp 2}\sin\theta_{i2}, \qquad \Delta\Phi = \pi. \tag{44}$$

Assuming symmetry, $\xi_1 = \xi_2$ and $\theta_{i1} = \theta_{i2}$, and eq. (43) shows that cross polarization is avoided if the two mirrors have equal concave curvature perpendicular to the plane of incidence and are close enough, $\Delta z \ll k\bar{\xi}^2$, or both far enough to one side or the other of the beam waist so that negligible "beam waist" phase shift takes place. From eq. (44), cross polarization can also be avoided if the reflectors are on opposite sides of the beam waist and in its far field, $\Delta z \gg k\bar{\xi}^2$, if one reflector is concave and the other convex with equal and opposite curvature normal to the plane of incidence.

Note, from eq. (41), if two identical reflectors are placed symmetrically about the beam waist in the far field, then $\gamma_1 = \gamma_2$ and $\Delta\Phi = \pi$ so the cross-polarization coupling is 6 dB higher than that resulting from just one of the reflectors.

Measurements made by K. C. Kelley[10] on a symmetrical dual-reflector beam-waveguide feed subsystem for a Cassegrainian antenna provide a valuable check on this theory for the combined effect of two of the factors, reflector curvature and longitudinal propagation length. An analysis of his 11-GHz measurements is given in the appendix. The reflectors had equal curvature, the beam size was nearly the same at both curved reflectors, and the relative phase shift was ap-

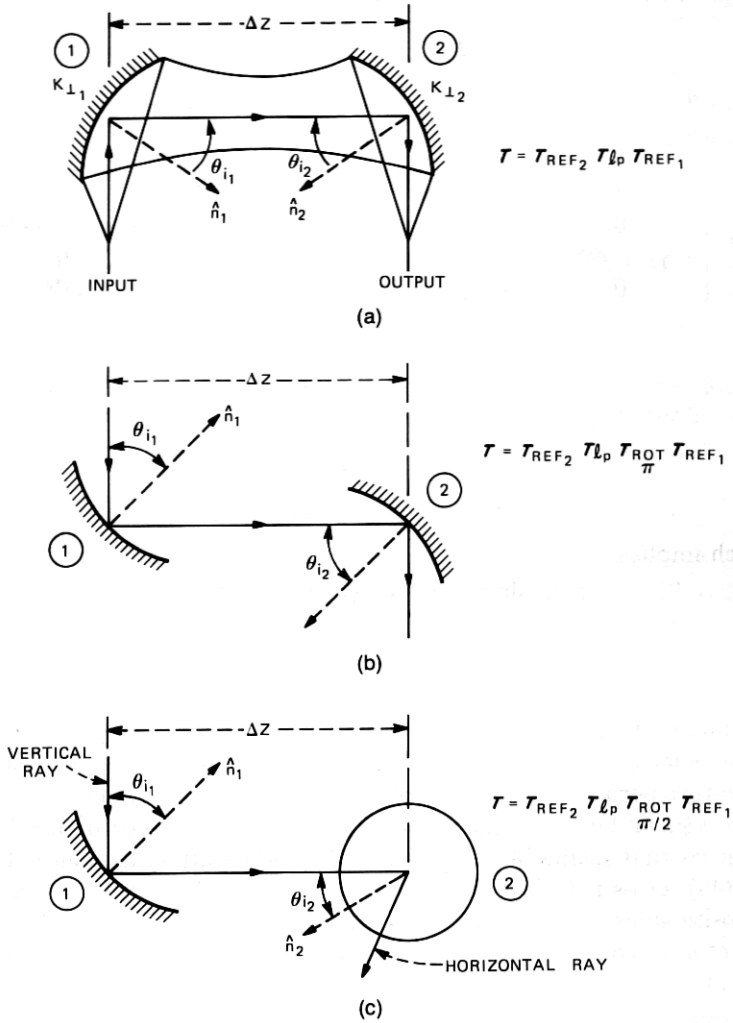

Fig. 8—Some typical beam waveguide applications. (a) Symmetrical dual reflector. (b) Asymmetrical dual reflector. (c) Right-angle dual reflector.

proximately 90 degrees between fundamental and higher-order modes. Thus, from eq. (41), the cross-polarization coupling of the pair at the center frequency is approximately 3 dB higher than that from a single reflector, as confirmed by the measurements. Also, the theoretical frequency dependence of cross-polarization coupling is in approximate agreement with the measurements as shown in the appendix and Fig. 13.

5.2 Asymmetrical dual reflector

In the asymmetrical dual reflector shown in Fig. 8b, the plane of incidence is rotated π radians. The overall matrix is the product of four beam factor matrices,

$$T = T_{\text{ref }2} T_{lp} T_{\text{rot }\pi} T_{\text{ref }1}, \tag{45}$$

where, from eq. (39), since $\beta = \pi$,

$$T_{\text{rot }\pi} = \begin{bmatrix} -1 & 0 & 0 & 0 \\ 0 & -1 & 0 & 0 \\ 0 & 0 & 1 & 0 \\ 0 & 0 & 0 & 1 \end{bmatrix}. \tag{46}$$

Thus (neglecting terms of order γ^2),

$$T = \begin{bmatrix} -1 & 0 & (\gamma_1 + e^{j\Delta\Phi}\gamma_2) & 0 \\ 0 & -1 & 0 & (\gamma_1 + e^{j\Delta\Phi}\gamma_2) \\ (\gamma_2 + e^{j\Delta\Phi}\gamma_1) & 0 & e^{j\Delta\Phi} & 0 \\ 0 & (\gamma_2 + e^{j\Delta\Phi}\gamma_1) & 0 & e^{j\Delta\Phi} \end{bmatrix}, \tag{47}$$

and the requirement that higher-order modes be avoided is

$$e^{-j\Delta\Phi} = -\frac{\xi_1 \kappa_{11} \sin\theta_{i1}}{\xi_2 \kappa_{12} \sin\theta_{i2}}. \tag{48}$$

Thus the conclusions stated above for the symmetrical dual-reflector configuration with equal (or opposite) curvature on reflectors 1 and 2 apply to the asymmetrical dual-reflector system with opposite (or equal) curvatures on reflectors 1 and 2, respectively.

Note, with closely spaced reflectors in the asymmetrical reflector arrangement ($\Delta z \to 0$, $\theta_{i1} = \theta_{i2}$), a pair of equal curvature mirrors give 6 dB more cross-polarization power coupling than just one of the mirrors, whereas oppositely curved mirrors give cancellation of cross polarization (a well-known property of the Cassegrainian reflector arrangement).

5.3 Right-angle dual reflector

In the right-angle dual reflector shown in Fig. 8c, the plane of incidence is rotated by $\pi/2$ radians. From eq. (39), with $\beta = \pi/2$, the matrix for rotation of the plane of incidence is

$$T_{\text{rot }\pi/2} = \begin{bmatrix} 0 & -1 & 0 & 0 \\ 1 & 0 & 0 & 0 \\ 0 & 0 & -1 & 0 \\ 0 & 0 & 0 & -1 \end{bmatrix}, \tag{49}$$

and the resulting overall matrix is (neglecting terms of order γ^2)

$$T = \begin{bmatrix} 0 & 1 & -e^{j\Delta\Phi}\gamma_2 & -\gamma_1 \\ -1 & 0 & \gamma_1 & -e^{j\Delta\Phi}\gamma_2 \\ -e^{j\Delta\Phi}\gamma_1 & -\gamma_2 & -e^{j\Delta\Phi} & 0 \\ \gamma_2 & -e^{j\Delta\Phi}\gamma_1 & 0 & -e^{j\Delta\Phi} \end{bmatrix}. \tag{50}$$

From eq. (50), it is seen that the cross polarization introduced by the first curved reflector cannot be cancelled by the second curved reflector in a right-angle dual-reflector system.

5.4 Confocal beam feed for an offset Cassegrainian antenna

As mentioned in the introduction, an attractive application of beam reflectors is as a feed for a satellite-system ground-station reflector antenna. To show how the above theory may be applied to multiple-reflector antennas, we consider the example of an offset Cassegrainian antenna fed by a beam waveguide. The offset Cassegrainian[11] configuration provides a main reflector aperture with little or no blockage and is shown in Fig. 9 along with a beam reflector feed path from the

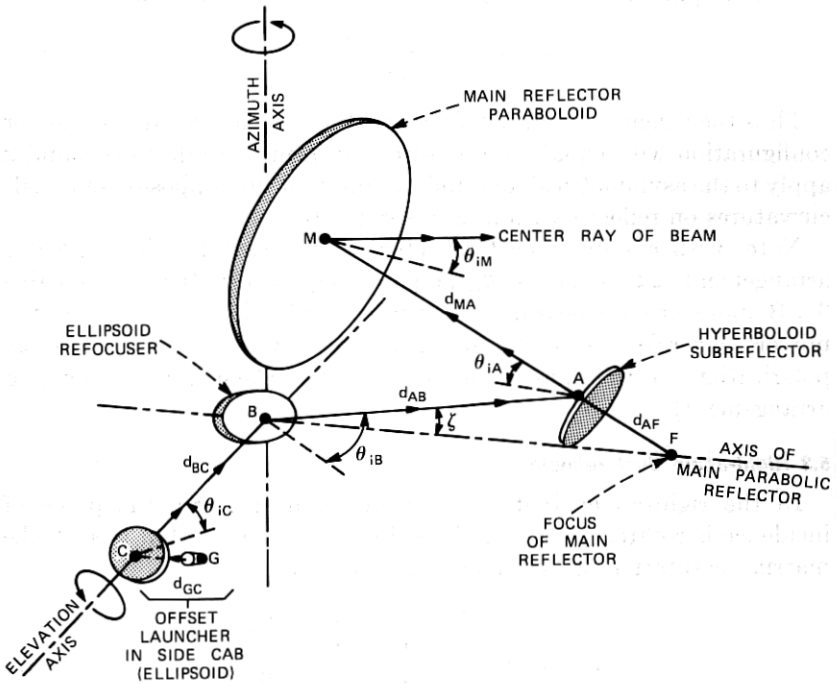

Fig. 9—Beam reflector feed for offset Cassegrainian antenna.

subreflector to a focusing reflector at the elevation axis and on out the elevation axis to an offset launcher[6] in a side cab.

We assume a confocal feed-reflector arrangement as suggested by Arnaud.[12] Subreflector A is an hyperboloid with foci at F and B, refocuser B an ellipsoid with foci at A and C, and the offset launcher reflector is an ellipsoid with foci at G and B. The advantage of this arrangement is that the beam diameters at A and C remain constant with frequency, as do the reflector curvatures, since the beam always seems to originate from the fixed points G, C, B, A, or F. This assumes the feed horn at G has constant beam width and phase center position over the range of frequency variation.

Tracing from G through the beam reflector system, we have the following factors: reflector C, longitudinal propagation length d_{BC}, plane of incidence rotation β_{BC}, reflector B, longitudinal propagation length d_{AB}, plane of incidence rotation $\beta_{AB} = -\pi/2$, reflector A, longitudinal propagation length d_{MA}, plane of incidence rotation $\beta_{MA} = \pi$, and reflector M. Thus the overall matrix

$$\boldsymbol{T} = \boldsymbol{T}_{\text{ref } M}\boldsymbol{T}_{\text{rot } \pi}\boldsymbol{T}_{lp\, d_{MA}}\boldsymbol{T}_{\text{ref } A}\boldsymbol{T}_{\text{rot } -\pi/2}\boldsymbol{T}_{lp\, d_{AB}}\boldsymbol{T}_{\text{ref } B}\boldsymbol{T}_{\text{rot } \beta_{BC}}\boldsymbol{T}_{lp\, d_{BC}}\boldsymbol{T}_{\text{ref } C}. \quad (51)$$

Since the cross polarization is small and we may neglect terms of second order ($\gamma^2 \ll 1$), it is easier to add the phasor higher-order mode coupling coefficients as one progresses through the system than to multiply out all the matrices shown in eq. (51).

$$\gamma_{VV} = \gamma_{HH} = -\{\gamma_M + \exp(j\Delta\Phi_{MA})\gamma_A + \sin\beta_{BC}\exp[j(\Delta\Phi_{MA} + \Delta\Phi_{AB} + \Delta\Phi_{BC})]\gamma_C\}, \quad (52)$$

$$\gamma_{VH} = -\gamma_{HV} = \exp[j(\Delta\Phi_{MA} + \Delta\Phi_{AB})][\gamma_B - \cos\beta_{BC}\exp(j\Delta\Phi_{BC})\gamma_C], \quad (53)$$

where, for example, γ_{VH} is the "normal to plane of incidence" output higher-order mode, when unit "parallel to plane of incidence" fundamental mode is present at the output, and

$$\Delta\Phi_{BC} = \arctan\left(\frac{z_B}{k\xi_{BC}^2}\right) - \arctan\left(\frac{z_C}{k\xi_{BC}^2}\right), \quad (54)$$

and

$$\gamma_B = 2\xi_B\kappa_{\perp B}\sin\theta_{iB}, \quad (55)$$

ξ_{BC} being the beam waist radius of the beam traveling from reflector C to reflector B, z_B, and z_C the longitudinal positions of reflectors B and C, respectively, relative to that beam waist, ξ_B the beam radius at reflector B, and $\kappa_{\perp B}$ the curvature of reflector B perpendicular to the plane of incidence.

The curvature in the plane perpendicular to the plane of incidence for quadric surfaces of revolution, with beam center rays passing

through the foci, may be shown to equal*

$$\kappa_\perp = \frac{a \cos \theta_i}{b^2}, \tag{56}$$

where a is the major axis, b the minor axis, and θ_i the angle of incidence of the beam center ray. Using eq. (56) and neglecting diffraction ($\Delta\Phi_{MA} \doteq 0$) between the subreflector A and the main reflector M, one finds that the cross-polarization coupling due to the Cassegrainian combination of M and A is

$$\gamma_{CASS} = \gamma_M + \gamma_A = \gamma_M \frac{\sin^2 (\zeta/2)}{\sin^2 \theta_{iM}}, \tag{57}$$

where ζ is the offset angle, relative to the main reflector axis of the beam center ray incident on the subreflector A. Equation (57) is just the result one would obtain from an equivalent parabola[13] with focal length $(e + 1)/(e - 1)$ times that of reflector M and with beam center ray offset angle ζ.

As frequency decreases from infinity, a beam waist appears on both sides of reflector B; however, $\Delta\Phi_{AB}$ and $\Delta\Phi_{BC}$ remain equal to $\pi/2$.[12] Because of this phase relation, it is not possible to cancel γ_B with γ_C in (53). However, the residual of $\gamma_M + \gamma_A$ in eq. (52) may be cancelled by a special choice of β_{BC}. In fact, if γ_C is adjusted to equal $\gamma_M + \gamma_A$, $\beta_{BC} = \pi/2$ will minimize the cross-polarized modes of both (52) and (53). To maintain $\beta_{BC} = \pi/2$, it is necessary to rotate the offset launcher in Fig. 9 as the antenna is rotated around the elevation axis, just as the fundamental mode polarization at the side cab launcher rotates with antenna elevation angle.

Thus, with $\Delta\Phi_{MA} \doteq 0$, $\gamma_c = \gamma_M + \gamma_A$, and $\beta_{BC} = \pi/2$, we have

$$\gamma_{VV} = \gamma_{HH} \doteq 0 \tag{58}$$

and

$$|\gamma_{VH}| = |\gamma_{HV}| = \gamma_B. \tag{59}$$

From (23) and (25) and $\theta_{iB} = 45°$,

$$\gamma_B = \xi_B \left(\frac{1}{d_{AB}} + \frac{1}{d_{BC}} \right) \tan \theta_{iB} = \frac{1 + d_{AB}/d_{BC}}{k\xi_A}. \tag{60}$$

To satisfy the condition on γ_c, we may choose an incidence angle, θ_{ic}, as follows, from eq. (57),

$$\xi_c \left(\frac{1}{d_{GC}} + \frac{1}{d_{BC}} \right) \tan \theta_{ic} = \gamma_M \frac{\sin^2 (\zeta/2)}{\sin^2 \theta_{iM}},$$

* Use the method of Ref. 4, Sec. 19.8, for example.

or

$$\tan \theta_{ic} = \frac{\tan (\zeta/2)}{(d_{BC}/d_{GC}) + 1}. \tag{61}$$

As a specific example to illustrate the cross polarization encountered in practice, consider the following typical antenna dimensions:

$$\frac{d_{AB}}{d_{BC}} = \frac{23}{14}, \quad \frac{d_{BC}}{d_{GC}} = \frac{14}{4}, \quad \zeta = 7.3°, \quad k\xi_A = 4f, \tag{62}$$

where f is the frequency in GHz. Thus, the cross-polarization coupling becomes

$$20 \log_{10} \left(\frac{\gamma_B}{\sqrt{e}} \right) = -8 - 20 \log_{10} f \text{ dB}, \tag{63}$$

e.g., -34 dB at 20 GHz. The incidence angle required on the offset launcher to cancel $\gamma_M + \gamma_A (= -54.3$ dB) in (52) becomes 1.6 degrees, which is too small to be practical without blockage, thus other means would be required to reduce γ_C; for example, the launcher could itself be an offset Cassegrainian antenna.

The cross polarization due to the ellipsoid refocuser at B can be reduced by using an additional flat mirror in combination[14] as shown in Fig. 10. With long focal lengths, the beam is essentially of constant width through the combination, and the resultant incidence angle allowing no beam blockage for a beam diameter D depends on the available space h,

$$\theta_{iB} = \frac{1}{2} \arcsin \left(\frac{D}{h} \right). \tag{64}$$

As a specific example, assume there is space available for $D/h = \frac{1}{3}$; whence θ_{iB} is reduced from 45 to 19 degrees and from eq. (60) the cross polarization is reduced 9 dB.

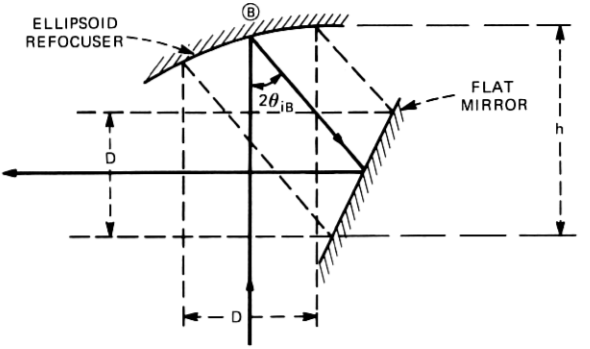

Fig. 10—Combination ellipsoid and flat to reduce θ_{iB}.

VI. CONCLUSIONS

By using the paraxial ray approximation, it has been possible to develop simple formulas for the cross polarization introduced by curved reflectors, e.g., eq. (12). The effect of curved reflectors in a beam-reflector configuration using quadric surfaces of revolution, with the beam center ray passing through the foci, is shown to be accurately characterized by two gaussian modes for each of two planes of polarization. Cross polarization in a general beam-reflector arrangement depends on three factors: reflector curvature, longitudinal propagation length, and rotation of plane of incidence. Using the gaussian modes allows one to represent the effect of the above factors by beam factor matrices which relate the input and output fundamental and higher-order gaussian modes. Some typical beam-reflector configurations were analyzed using these techniques. The theory agrees well with measurements on single reflectors,[6] on a symmetrical dual-reflector system,[10] and with numerical ray tracing computations.

There has been considerable interest in the effect of reflector curvature in beam-reflector configurations. In particular, the work by Mizusawa and Kitsuregawa[15] is worth noting. They show that the symmetric amplitude distribution of an optical beam passing through the foci of a pair of quadric surface-of-revolution reflectors will be preserved if all the foci lie on a straight line and if the eccentricities of the two reflectors are properly related. If both reflectors are ellipsoids or both reflectors are hyperboloids, then the eccentricities must be equal and the exit beam will be parallel to the entrance beam. If one reflector is an ellipsoid and one reflector is an hyperboloid, then one eccentricity must be the inverse of the other eccentricity and the direction of the exit beam is the reflection around the line through the foci of the direction of the entrance beam. By using eq. (12), one can show that only in the case of equal eccentricities does the preservation of amplitude symmetry imply zero cross polarization and then only in the infinite frequency limit where beam waist diffraction is negligible so the relative phase shift between fundamental and higher-order modes is either 0 or 180 degrees.

The frequency dependence of the cross-polarization coupling in a beam-reflector system is an important property not generally indicated in the literature. The paraxial ray approximation for beam diffraction used herein provides a convenient means for computing the frequency dependence of the cross-polarization coupling which, in some cases, can be quite strong; e.g., in eq. (63) for the reflector configuration of Fig. 9 the cross-polarized power varies as the inverse square of the frequency.

VII. ACKNOWLEDGMENTS

It is a pleasure to acknowledge A. A. M. Saleh, D. C. Hogg, and E. A. Ohm for many helpful discussions and J. A. Arnaud for descriptions of Hertzian cable dual-reflector refocusers and confocal triple-reflector arrangements.

APPENDIX

Comparison of the Matrix Theory With Measurements on a Beam Waveguide

The measurements described in Ref. 10 involved a beam-waveguide feed for a Cassegrainian antenna arranged as shown in Fig. 11. Reflectors 9a and 9c are identical ellipsoids approximately 0.76 m by 1.09 m in size with major and minor axes $a = 3.656$ m and $b = 3.656$ m/$\sqrt{2}$, respectively. Reflectors 9b and 9d are flat mirrors. When one uses the images of the flat mirrors to unfold the beam waveguide, it is seen that a symmetrical dual-reflector type results as shown in Figs. 8a and 12. The feed was designed to produce beam waists approximately at planes u-u and v-v of Fig. 11 and a beam of the proper diameter and phase curvature at the subreflector position w-w to provide a focussed wave reflected from the subreflector toward the main reflector (not shown) of the Cassegrainian antenna. Performance for both vertical and horizontal polarization was measured by rotating the launching horn (No. 8 of Fig. 11) around its axis (azimuth axis). Measurements were made at 10.36, 11.06, and 11.76 GHz for both horn polarizations. The phase and amplitude of the copolarized signal at the subreflector position was measured along the intersection line of plane w-w and the beam-bending plane (the plane of the paper in Fig. 11), and the cross-polarized signal (at plane v-v) along a line in the beam-bending plane and also along a line perpendicular to the beam-bending plane. The cross-polarized signal along the line in the beam-bending plane always remained below -40 dB relative to the on-axis copolarized signal.

To compare these measurements with theory, the launching horn is assumed to radiate negligible cross-polarized signal and, since measurements of the beam dimensions throughout the reflector system are not available, the beam measurements at the subreflector position (plane w-w) will be used to reconstruct the beam dimensions throughout the beam waveguide as shown in the following equations. The theoretical cross polarization will then be computed at plane v-v and compared with measurements.

Since the horn did not produce a perfectly symmetrical gaussian beam, the average (over both horn polarizations) of the measurements at planes w-w and v-v are used in the gaussian beam analysis. From the

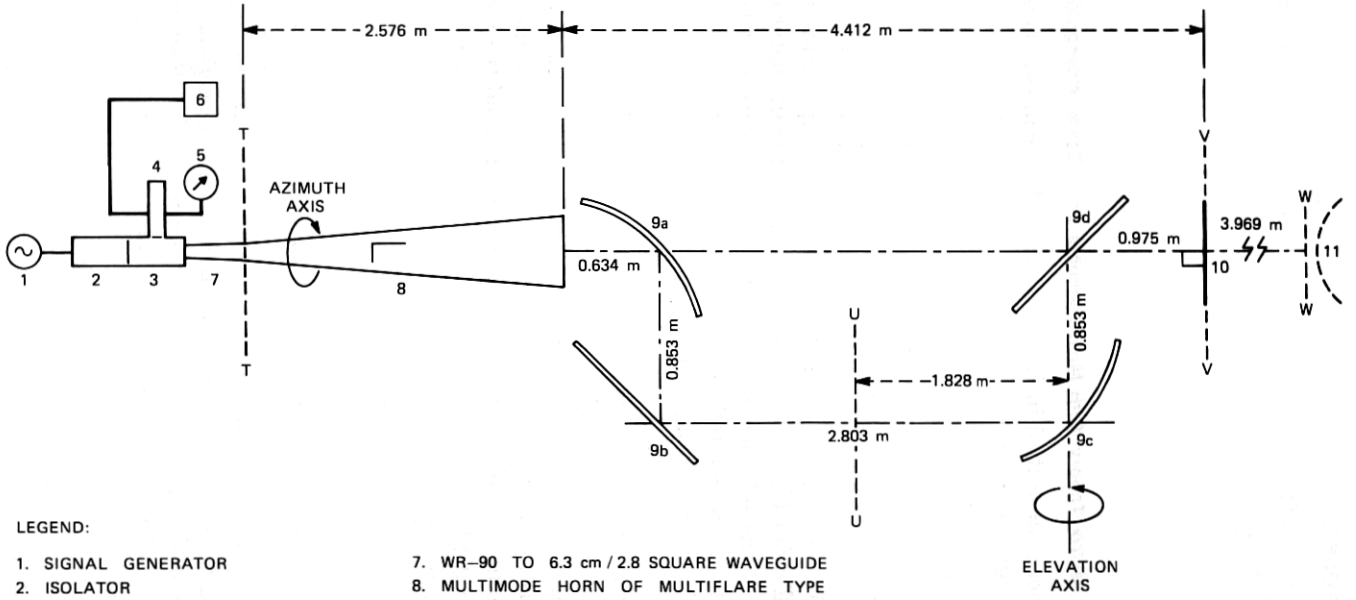

LEGEND:

1. SIGNAL GENERATOR
2. ISOLATOR
3. WR–90 SLOTTED LINE
4. PROBE
5. PROBE POSITION DIAL INDICATOR
6. STANDING WAVE INDICATOR
7. WR–90 TO 6.3 cm / 2.8 SQUARE WAVEGUIDE
8. MULTIMODE HORN OF MULTIFLARE TYPE
9. REFLECTORS OF FOLDED BEAM WAVEGUIDE SUBSYSTEM
10. FLAT ALUMINUM PLATE SHORT THROUGH PHASE CENTER OF FINAL IMAGE
11. POSITION CORRESPONDING TO SUBREFLECTOR OF CASSEGRAINIAN ANTENNA

Fig. 11—Experimental setup for measurement of subsystem total loss.

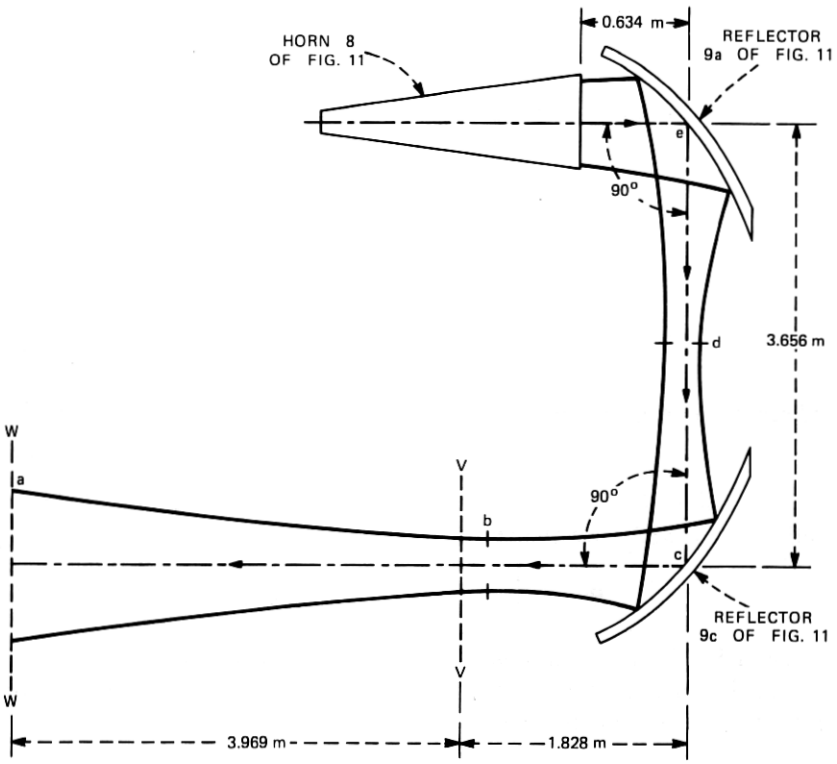

Fig. 12—Unfolded beam waveguide.

measurements at plane w-w, the gaussian beam radius ξ_a and phase front radius of curvature R_a at the subreflector position are given in Table I.

Using the beam transformation formulas of Ref. 8, the beam radius, ξ_b, at the beam waist b and the distance from the subreflector to the beam waist z_{ab} are

$$\xi_b = \frac{\xi_a}{\sqrt{1 + (k\xi_a^2/R_a)^2}} \tag{65}$$

Table I — Measured gaussian beam parameters at the subreflector position

Frequency (GHz)	Beam Radius (meters) ξ_a	Phase Front Radius of Curvature (meters) R_a
10.36	0.355	4.177
11.06	0.328	4.623
11.76	0.338	5.027

and

$$z_{ab} = \frac{R_a}{1 + (R_a/k\xi_a^2)^2}, \tag{66}$$

where $k = 2\pi/\lambda$ is the free-space propagation constant.

Going from beam waist b in Fig. 12 to reflector 9b at c, the transformation formulas give the beam parameters on the output side of the reflector,

$$\xi_c = \xi_b \sqrt{1 + \left(\frac{z_{bc}}{k\xi_b^2}\right)^2} \tag{67}$$

and

$$R_{c_{\text{out}}} = z_{bc}\left[1 + \left(\frac{k\xi_b^2}{z_{bc}}\right)^2\right], \tag{68}$$

where z_{bc} is the distance from beam waist b to reflector c in Fig. 12,

$$z_{bc} = 5.797 - z_{ab} \text{ meters}. \tag{69}$$

The radius of curvature of the beam phase front on the input side of reflector c is given by the thin lens formula[9]

$$R_{c_{\text{in}}} = \left[\frac{1}{1.828} - \frac{1}{R_{c_{\text{out}}}}\right]^{-1} \text{meters}, \tag{70}$$

where 1.828 is the focal length of the ellipsoidal reflectors.

The beam radius ξ_d at the beam waist d and the distance from reflector c to the beam waist z_{cd} are

$$\xi_d = \frac{\xi_c}{\sqrt{1 + (k\xi_c^2/R_{c_{\text{in}}})^2}} \tag{71}$$

and

$$z_{cd} = \frac{R_{c_{\text{in}}}}{[1 + (R_{c_{\text{in}}}/k\xi_c^2)^2]}. \tag{72}$$

The beam radius at reflector e (9a) is

$$\xi_e = \xi_d \sqrt{1 + \left(\frac{z_{de}}{k\xi_d^2}\right)^2}, \tag{73}$$

where the distance from beam waist d to reflector e is

$$z_{de} = 3.656 - z_{cd} \text{ meters}. \tag{74}$$

From Section 5.1, the maximum cross-polarized signal at plane v-v occurs perpendicular to the beam-bending plane at a distance ξ_v from the axis, where ξ_v is the beam radius at plane v-v

$$\xi_v = \xi_b \sqrt{1 + \left(\frac{z_{bv}}{k\xi_b^2}\right)^2}, \tag{75}$$

and the distance from the beam waist b to plane v-v is

$$z_{bv} = z_{ab} - 3.969 \text{ meters}. \tag{76}$$

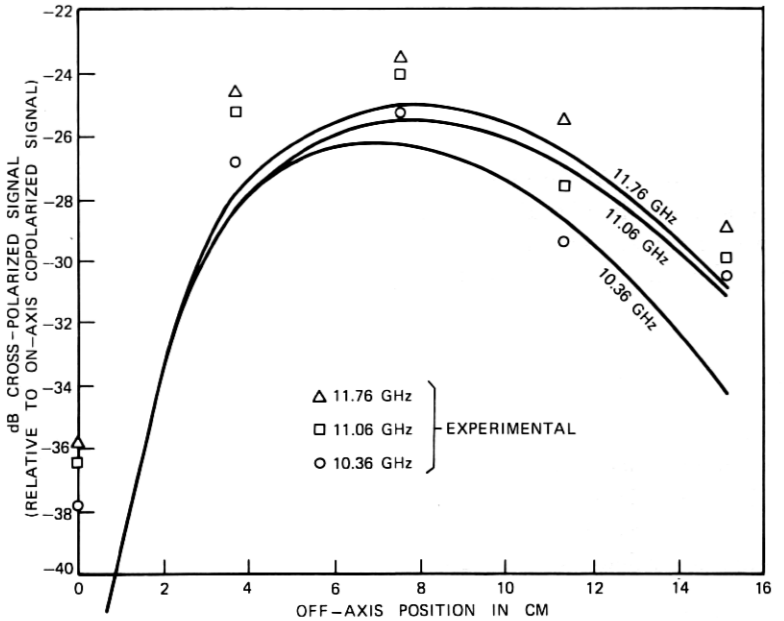

Fig. 13—Comparison of theoretical and measured cross-polarization signal at plane *V-V*.

From eq. (41), the maximum cross-polarized signal amplitude relative to the on-axis copolarized signal is

$$C_{\max} = \frac{-\gamma_c + e^{j\Delta\Phi}\gamma_e}{\sqrt{e}}, \tag{77}$$

where the mode coupling coefficient at reflector c is

$$\gamma_c = 2\xi_c\kappa_{1c} \sin\theta_{i_c} = \frac{\xi_c}{1.828}, \tag{78}$$

because the incidence angle $\theta_{i_c} = 45$ degrees and the curvature is $\kappa_{1c} = (a/b^2)\cos\theta_{i_c}$ (a and b are the major and minor axes of the ellipsoid, respectively). Similarly,

$$\gamma_e = \frac{\xi_e}{1.828}. \tag{79}$$

$\Delta\Phi$ is the relative phase shift of the higher-order mode relative to the fundamental mode over the longitudinal propagation length between reflectors c and e; from eq. (38),

$$\Delta\Phi = \arctan\left(\frac{|z_{cd}|}{k\xi_d^2}\right) + \arctan\left(\frac{|z_{de}|}{k\xi_d^2}\right). \tag{80}$$

From eq. (18), to find the cross-polarized field at any other radius ρ

instead of $\rho_{c_{\max}} = \xi_v$, one multiplies by the factor:

$$C(\rho) = C_{\max} \left\{ \frac{\rho}{\xi_v} \exp \left[(1 - \rho^2/\xi_v^2)/2 \right] \right\}. \tag{81}$$

Using eqs. (65) through (81) and the values given in Table I, the curves shown in Fig. 13 were computed for the cross-polarized signal power (relative to on-axis copolarized signal) as a function of distance from the axis at plane v-v in a direction perpendicular to the beam-bending plane for the three frequencies 10.36, 11.06, and 11.76 GHz. Also shown are the measured values from Ref. 10. The theory is in approximate agreement with the measurements, showing the shape of the curve of cross-polarized signal versus off-axis distance and approximating the absolute level of the maximum cross-polarized signal. The frequency dependence of the theoretical cross-polarized signal is also in the same direction as the measured values.

Theoretically, the cross polarization in the beam-bending plane is negligible, which also is in agreement with the measurements.

REFERENCES

1. D. C. Hogg and R. A. Semplak, "An Experimental Study of Near Field Cassegrainian Antennas," B.S.T.J., *43*, No. 6 (November 1964), pp. 2677–2704.
2. J. A. Arnaud and J. T. Ruscio, "Guidance of 100-GHz Beams by Cylindrical Mirrors," IEEE Trans. on Microwave Theory and Techniques, *MTT-23*, No. 4 (April 1975), pp. 377–379.
3. G. Goubau and F. Schwering, "On the Guided Propagation of Electromagnetic Wave Beams," IRE Trans. on Antennas and Propagation, *AP-9*, No. 3 (May 1961), pp. 248–256.
4. H. S. M. Coxeter, *Introduction to Geometry*, New York: John Wiley, 1969, Secs. 19.4 and 19.5.
5. C. Dragone, "An Improved Antenna for Microwave Radio Systems Consisting of Two Cylindrical Reflectors and a Corrugated Horn," B.S.T.J., *53*, No. 7 (September 1974), pp. 1351–1377.
6. M. J. Gans and R. A. Semplak, "Some Far-Field Studies of an Offset Launcher," B.S.T.J., *54*, No. 7 (September 1975), pp. 1319–1340.
7. J. A. Arnaud and J. T. Ruscio, "Focusing and Deflection of Optical Beams by Cylindrical Mirrors," Appl. Opt., *9*, No. 10 (October 1970), pp. 2377–2380.
8. H. Kogelnik and T. Li, "Laser Beams and Resonators," Appl. Opt., *5*, No. 10 (October 1966), pp. 1550–1567.
9. S. Ramo, J. R. Whinnery, T. VanDuzer, *Fields and Waves in Communication Electronics*, New York: John Wiley, 1965, Sec. 11.09.
10. K. C. Kelley, "Test Data Report for Rantec Model ASF-122 Feed Subsystem," Rantec Proposals No. 62001-TR, April 7, 1972 and No. 6200-TR-1, May 17, 1972.
11. C. Dragone and D. C. Hogg, "The Radiation Pattern and Impedance of Offset and Symmetrical Near-Field Cassegrainian and Gregorian Antennas," IEEE Trans. on Antennas and Propagation, *AP-22*, No. 3 (May 1974), p. 472.
12. J. A. Arnaud, private communication, November 27, 1970.
13. P. W. Hannan, "Antennas Derived from the Cassegrain Telescope," IRE Trans. on Antennas and Propagation, *AP-9*, March 1961, pp. 140–153.
14. D. C. Hogg, private communication, January 30, 1974.
15. M. Mizasawa and T. Kitsuregawa, "A Beam-Waveguide Feed Having A Symmetric Beam for Cassegrain Antennas," IEEE Trans. on Antennas and Propagation, *AP-21*, No. 6 (November 1973), pp. 884–886.